Hydrothermally Synthesized Sulfur-Doped Graphite as Supercapacitor Electrode Materials

Hydrothermally Synthesized Sulphur Doped Graphite as Supercapacitor Electrode Materials

Sayantan Maity,[a] Debosmita Banerjee,[b] Gourav Bhattacharya,[c] Susanta Sinha Roy,[b]* Basab Bijayi Dhar[a]*

[a]Department of Chemistry, School of Natural Sciences, Shiv Nadar University, Gautam Buddha Nagar, Dadri, UP-201314, India
[b]Department of Physics, School of Natural Sciences, Shiv Nadar University, Gautam Buddha Nagar, Dadri, UP-201314, India
[c]School of Engineering, Ulster University, Newtownabbey, Belfast BT37 0QB, Northern Ireland, United Kingdom

Email for correspondence: susanta.roy@snu.edu.in; basabbijayi@gmail.com, basab.dhar@snu.edu.in

Keywords: Sulphur-doped graphite, Porous material, Hydrothermal method, Supercapacitor, Electrochemical Impedance Spectroscopy

Abstract

Sulphur-doped Graphite (S-DG) was synthesized using a sustainable method. Low-cost cellulose fibre and carbon disulphide (CS_2) were used as the precursor for a carbon source and a sulphur source respectively and a multistep chemical and thermochemical synthesis process was employed to obtain S-DG. Advanced microscopic and spectroscopic techniques and porosimetry analyses were performed to probe the surface morphology, surface area, microstructures, and chemical bonding states of S-DG. Interestingly, X-ray photoelectron spectroscopy reveals S-load was 3.81 atm% and 7.02 atm%, when the reactions were carried out in aqueous and dimethyl sulphoxide (DMSO) medium respectively. The specific surface area was calculated as 522.77 m^2g^{-1} and 693.27 m^2g^{-1} for the two materials. To our best knowledge, 7.02 atm% S-load is the highest S-doping reported so far in graphite material, where the laboratory chemicals have been used as precursors. Both the materials, i.e S-DG_{Water} and S-DG_{DMSO} were tested as supercapacitor electrode material in a portable electrochemical cell with a three-electrode system to check their potential and stability for the fabrication of renewable energy storage devices. Cyclic voltammetry (CV) and galvanostatic charging-discharging (GCD) techniques were performed within a potential window 1 V in presence of 1(M) Na_2SO_4 as electrolyte. Maximum specific capacitance (C_{Sp}) of S-DG_{Water} and S-DG_{DMSO} were obtained as 155.61 Fg^{-1} and 261.43 Fg^{-1} (at scan rate 10 mVs^{-1}) respectively. The result concluded that the extent of S-doping appeared as the key factor for controlling the peak current. Importantly, our investigation suggests that the sulphur in graphite facilitates a diffusion-driven storage mechanism and a higher amount of sulphur may enhance surface controlled storage as well. Both the materials show excellent cyclic stability with >98% retention of initial specific capacitance over 10000 cycles of charging-discharging.

1. Introduction

In recent years, the electrochemical supercapacitor (ESC) has gained huge attention due to its high power density, ultrafast charging-discharging capability, and long-life cycle. Based on the charge storage mechanism, ESC is classified into Electrical Double-Layer

Capacitor (EDLC) and Pseudocapacitor (PC).[1-4] Carbon-based materials are normally used to fabricate EDLC and metal-based materials, functionalized polymers, or porous organic frameworks are used for PC.[1-2] However, in presence of any oxidizable or reducible functional groups in carbon-based material's framework, the materials can impart pseudocapacitive behaviour.[3] PC produces a much higher Faradaic current, but EDLC can be considered more advantageous in terms of its reversible charging-discharging and storage capacity for non-Faradaic electrical mechanisms.[2]

Porous carbon materials (PCM) derived from carbohydrates like glucose,[3] fructose,[4] xylose[5,] etc or biomass[6, 7] through hydrothermal treatment, have been excelled as extraordinary supercapacitor electrode materials. On the other hand, heteroatom doping at PCM can significantly change its electronic property and surface morphology to facilitate the charge transport and charge accretion at electrolyte-electrode interface.[3, 8-12] Boron (B),[9] nitrogen (N)[10] and several dual-doped[11] graphitic materials have widely been used as promising supercapacitor electrode materials. Compared to the smaller atoms, employment of sulphur (S)-doped graphite as ESC electrode material is less reported for the difficulty of larger atom incorporation.[12] The presence of S inside the carbon scaffolds can increase the polarizability and electrode-electrolyte wettability more than the other dopants.[12] Zhang *et al.* synthesized N, S dual doped mesoporous carbon materials by carbonizing the reaction mixture of pyrrole, absolute alcohol, and H_2SO_4. They have shown that, with the elevation of annealing temperature (650ºC to 950ºC), atm% of N decreased and atm% of S increased leading to better capacitive behaviour.[13] Very recently, Hamed *et al.* demonstrated a comparative study between N-doped and N, S-dual doped rGO where the capacitive behaviour of the later enhanced 2.5 times than the former.[14] Parveen *et al.* showed S-doping took place in graphene during electrochemical exfoliation of a graphite rod in presence of $Na_2S_2O_3$ and H_2SO_4 and due to S incorporation supercapacitor performance enormously.[15] Z. S. Wu *et al.* developed a 2D S-doped graphene thin film from an S-rich organic supramolecule and used it as a promising micro-supercapacitor (MSC), although its synthesis, as well as fabrication, took a long time.[16] All of these S-doped PCMs imparted PC-type behaviour. It happens generally because the presence of a much larger heteroatom boosts Faradaic current to a large extent.[12, 15] Apart from the laboratory chemicals,[15-18] biomass,[19-20] industrial and agricultural waste[21] are also used for the synthesis of S-doped PCM for sustainable development. However, in most of the cases, prolonged processing was required with harsh conditions. Besides, it led to uncontrolled dopant

entry, as N-doping also took place along with S.[20-21] Therefore, selective S doping in PCM is highly desirable using greener and cheaper chemicals following a relatively mild condition.

In the present work, we have synthesized Sulphur-doped graphite (S-DG) *via* a bottom-up approach using cellulose and carbon disulphide (CS_2) as the main precursors. The dopant amount was varied by changing the solvent and the supercapacitor performance of the material increased enormously with the amount of S. We have used 1(M) Na_2SO_4 as an electrolyte. Despite a high level of S-doping, the material restrained EDLC type behaviour. To compare the supercapacitor activity, we repeated the experiments with 1(M) H_2SO_4 and 1.5(M) NaOH which resulted in pseudocapacitive (PC) behaviour of S-DG to some extent. Three electrode system was used for the electrochemical experiments. Cyclic stability of the material was checked up to 10000 cycles.

2. Experimental section

2.1. Material synthesis

To synthesize S-DG, cellulose, a most-abundant biopolymer was chosen as the source of graphite (Scheme 1). In the first step, 100 mg cellulose was treated with excess carbon disulphide (CS_2) in a basic medium (5% NaOH) for 1 hour at room temperature (RT). During this process, a considerable amount of xanthate groups [-OC(S)-S^--] got attached to the -OH linkage of cellulose moiety. Sodium ions (Na^+) remained as the counter cations and one molecule of H_2O was eliminated per xanthatization. An orange colouration of the solution confirmed this transformation (Figure S1). Then the solution was filtered and the unreacted cellulose portion was discarded. This step is called the 'viscose' process in the industry and is usually followed by acid treatment in the textile industry to split out the xanthate group for the preparation of modified forms of cellulose like cellophane, viscose, rayon, lyocell, etc.[22] In the second step, 'Leuckart thiophenol synthesis', another industrially important reaction for the preparation of aryl thioesters and aryl thiols was carried out to replace the Na^+ from cellulose xanthate.[23] Excess amount of diazonium salt of sulphanilic acid was added to the dark orange solution of sodium cellulose xanthate and heated at 70 ^oC for 2 hours (hr). The diazonium salt of sulphanilic acid was chosen preferably to incorporate extra sulphur. The solution was cooled at RT and a dark brown solid was precipitated (Figure S2). This time, the filtrate was discarded and the residue was washed with cold water and diethyl ether repeatedly to remove both the unreacted reactants.

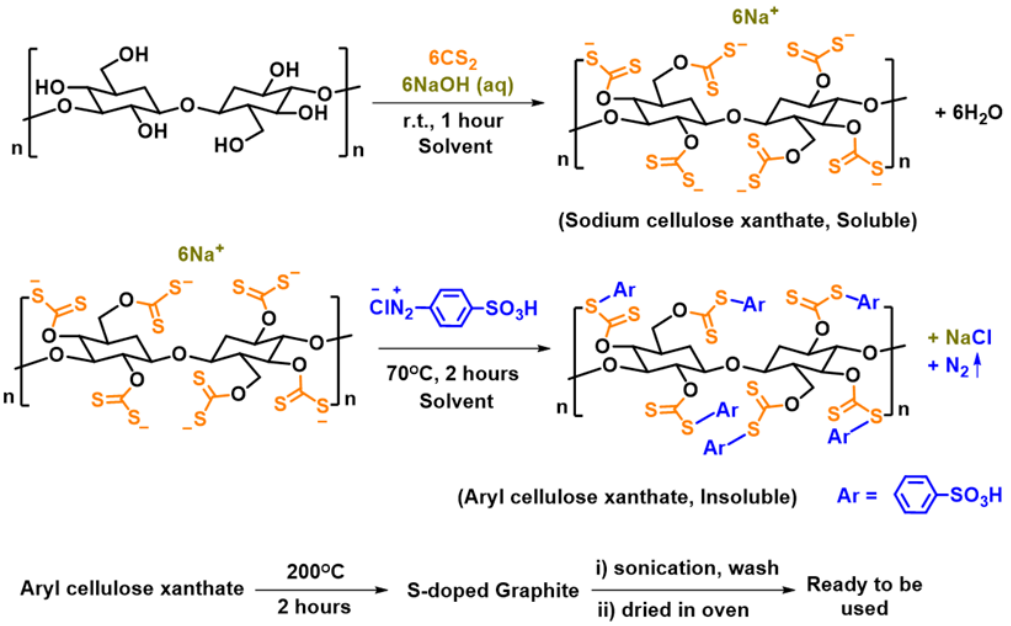

Scheme 1. Synthetic scheme of S-doped Graphite (S-DG).

It should not be expected that all the -OH would be replaced by -CS_2Na in the 1st step and all the -Na by -Ar in the second step. Hence, washing is very crucial here to remove all the unreacted base and sodium cellulose xanthate, so that no metal (Na) can stay in the final product. Finally, aryl cellulose xanthate was heated hydrothermally in a muffle furnace at 200^{o}C for 2 hr, inside a teflon container encapsulated in a tightly-sealed steel bomb-reactor under high pressure. The black charred materials were collected after cooling down the temperature and cleaned under ultrasound and dried in an oven.

We performed step one and step two in DMSO also as CS_2 is highly soluble in DMSO (45 g in 100 g at 20^{o}C) compared to water (2.17 g in 1 kg at 20^{o}C). This could be helpful for inserting more sulphur in cellulose. Apart from solubility, there were two more reasons for choosing DMSO. First, due to its high boiling point, it can tolerate heat in the hydrothermal process. Second and most vital, there is a possibility of extra S inclusion in the S-DG. DMSO was already reported to turn into S-doped Graphene as a single precursor under solvothermal treatment[24] by heating over 500^{o}C. In presence of DMSO in step 1, cellulose solution was converted to a dark brown solution which was highly viscous (Figure S1b). This might be due to the growth of oligo (oxymethylene) chains which can be cross linked to each other.[25] The step 1 was also carried out in toluene, which has high boiling point, but the cellulose xanthate was almost insoluble in toluene. Dimethyl formamide (DMF), which is also a high b.p. solvent, can readily solubilize CS_2 and cellulose-derived materials, forming a dense solution similar to

DMSO. However, it was avoided because N-doping can be possible due to the presence of DMF.[24]

Sodium cellulose xanthate and aryl cellulose xanthate were characterized through UV-Vis (Cary 8454 UV-Vis spectrophotometer) and FT-IR spectroscopy (Thermo Fisher Scientific Nicolte iS5 FTIR spectrometer, diamond ATR mode). The synthesized graphitic materials were named as S-DG_{Water} and S-DG_{DMSO}. The carbonization process from aryl cellulose xanthate was also monitored in FT-IR spectroscopy. The extremely high temperature for the carbonization was avoided so that the S-atoms can remain properly 'doped' inside graphite framework rather than forming elemental S-nanoparticles.[26]

2.2. Material Characterizations

The surface morphology of both the materials was characterized through Field Emission Scanning Electron Microscope (FESEM) in a Nova Nano SEM 450 (FEI), with gold coating. High-Resolution Transmission Electron Microscopic (HRTEM) analysis was done on Cu-grid at an accelerating voltage of 200 kV (TALOS S-FEG). Powder X-Ray Diffraction (P-XRD) was performed in Bruker discover-d8 instrument using Cu-K_α as the energy source (λ = 1.542 Å). Raman spectrum was recorded in an STR Raman spectrometer equipped with a 532 nm argon-ion laser source with 2.5 mW power and a 50x magnification objective lens. Brunauer-Emmett-Teller (BET) surface area and porosimetry analysis were performed in a Quantachrome autosorb automated gas sorption system. N_2 gas was chosen as the adsorbent at 77 K within the relative pressure range 0.05 to 1.0. The X-Ray Photoelectron Spectroscopy (XPS) was recorded in ESCA, Omicron Nanotechnology, Oxford Instrument. Taking the maximum intensity of the C 1s signal at 284.8 eV as the reference, the binding energies were calculated.

2.3. Electrode Preparation and Electrochemical Measurements

The electrochemical cell was set up with a three-electrode system, attached to a potentiostat (Biologics, SP-300). A glassy carbon electrode (GCE) was chosen as the working electrode (WE). Before drop-casting, its highly conductive surface was polished by rubbing with alumina slurry (0.05 μm mesh size) on a micro-cloth pad and cleaned with methanol in an ultrasonic bath for at least half an hour. After that, it was dried in an oven. S-DG was dispersed into millipore water at 0.2 mg/ml concentration and the suspension was made almost uniform after prolonged ultrasound treatment with a probe sonicator (VC505, Sonics & Materials, INC) at 10 kHz frequency. Then GCE surface was modified by drop-casting of 10

μl of the dispersed solution. After drop-casting, GCE was dried inside an oven at 60^{o}C for 4-5 hours (hrs), and then it would be ready for the electrochemical measurement. Periodic cleaning, drop-casting, and drying were essential before each experiment. Pt-wire was selected as the counter electrode (CE) and Ag/AgCl in presence of 3(M) KCl was selected as the reference electrode (RE). Cyclic voltammetry (CV) and galvanostatic charging-discharging (GCD) experiments using both of the materials were performed within a 1V potential window (0 to 1V) taking 1(M) Na_2SO_4 as electrolyte. Electrochemical Impedance Spectroscopy (EIS) was done within a frequency range from 100 mHz to 100 kHz. Total charge analysis of both doped and undoped graphite was plotted with the help of Density Functional Theory (DFT) using Gaussian code to understand the charge distribution through graphitic layer due to heteroatom-doping.

3. Results and discussion

Characterizations of sodium cellulose xanthate and aryl cellulose xanthate through UV-Vis and FT-IR are discussed in SI (Figure S3 and S4 respectively, Page S4 - S5). The *in-situ* carbonization was described in Figure S5. Characterizations of S-DG_{water} and S-DG_{DMSO} are discussed in this section.

3.1. Materials and Characterization

3.1.1. FESEM

FESEM images of S-DG_{Water} (Figure 1) and S-DG_{DMSO} (Figure 2) revealed the highly porous structure and irregular grain boundaries.[16] Micro-slits over the surface were observed in images of 500 nm magnification (Figure 1b, 1d, 2b, 2d). From the elemental mapping, more S-contain in S-DG_{DMSO} (Figure 2h) than S-DG_{Water} (Figure 1h) was observed. At the same time, the distribution of S was more homogeneous in S-DG_{DMSO}.

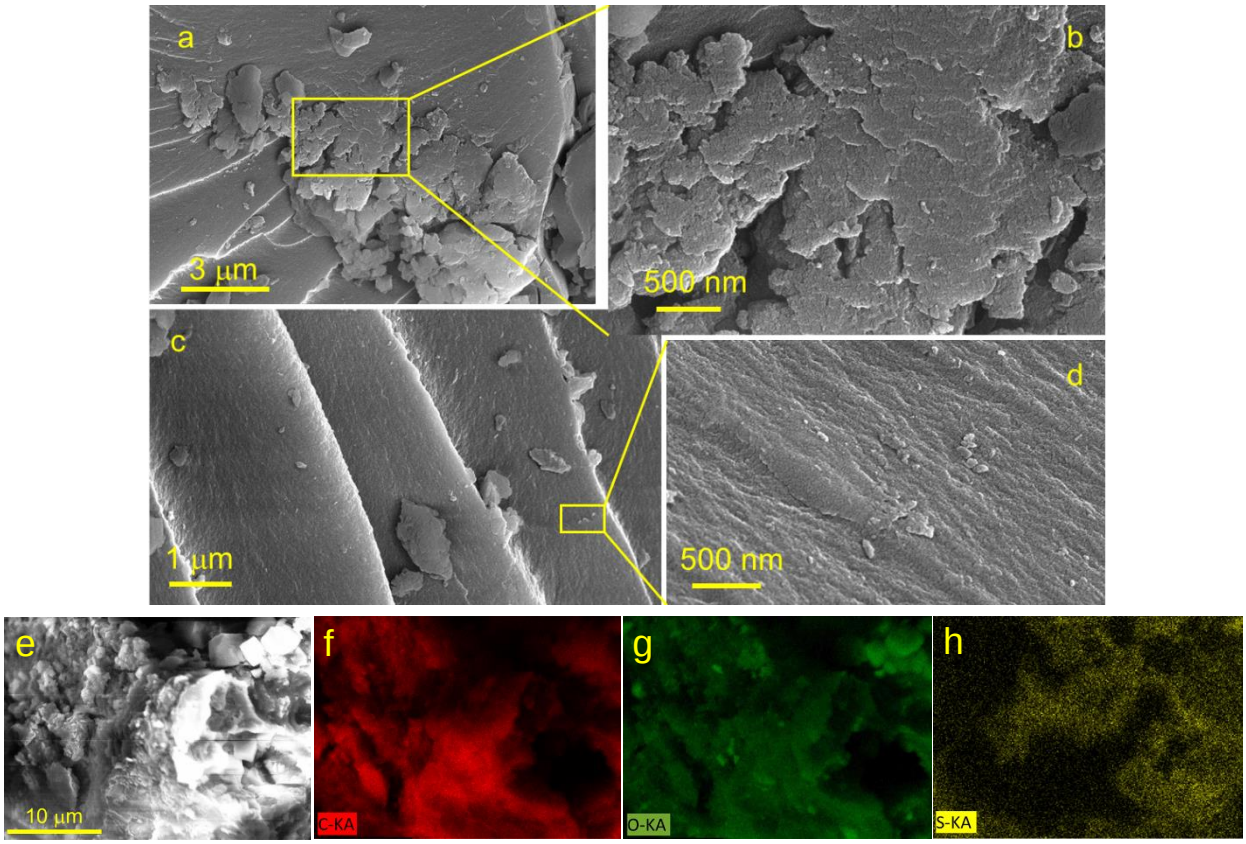

Figure 1. (a-d) FESEM images of S-DG_{Water}. (f-h): elemental mapping of C, O and S of the selected area shown in (e).

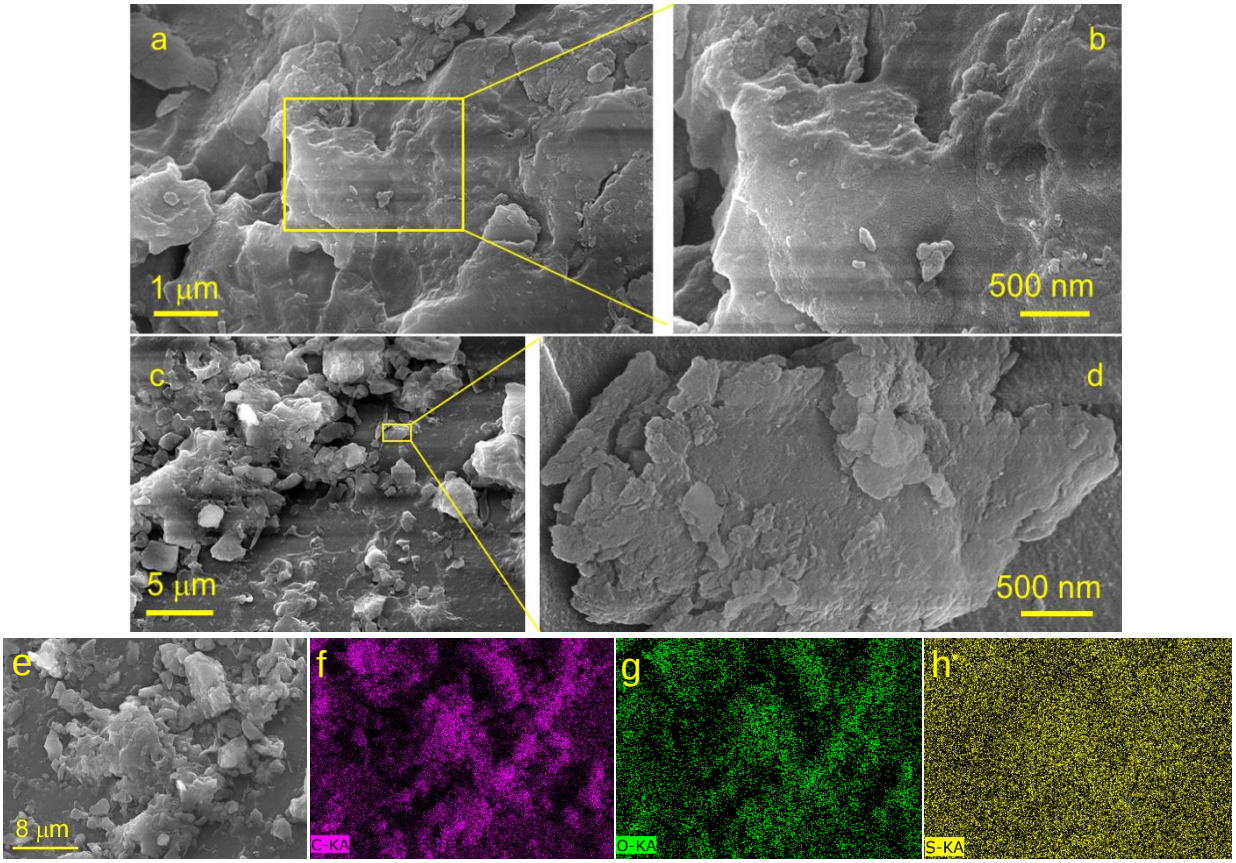

Figure 2. (a-d) FESEM images of S-DG_{DMSO}. (f) to (h): elemental mapping of C, O, and S of the selected area shown in (e).

3.1.2. HRTEM

TEM images (Figure S6 and S7) revealed that both of the materials are amorphous.[8] The randomly distributed black regions were observed for the uneven agglomeration of the graphitic layers.[15] From the irregular fringes of graphitic layers, interlayer distances were calculated using ImageJ software (Figure S6.e and Figure S7.c, i.e. images of 20 nm resolution). Diffused rings in the Selected Area Electron Diffraction (SAED) pattern (Figure S6.c and Figure S7.d) further signified the amorphous layers. All the S functionalities were covalently attached to the graphite as no crystalline sulphur nanoparticle (SNP) was observed.

3.1.3. P-XRD

The characteristic peak for graphite plane 002 was observed at 2θ = 23.21 for S-DG_{Water} and 22.54 for S-DG_{DMSO} respectively, in the P-XRD pattern (Figure S8).[24, 27] Interlayer spacing (d) was calculated using Bragg's law (Equation 1) and the values (3.82 Å and 3.95 Å) almost matched with the same obtained from HRTEM (3.78 Å and 3.97 Å). The slightly higher d-spacing for S-DG_{DMSO} over S-DG_{Water} was invariably due to the presence of more S-atoms. The mean size of the ordered crystalline domain or 'Correlation length' (τ) was calculated from Full Width Half Maxima (FWHM) for the graphitic peak using Scherrer's formula (Equation 2). This was less in S-DG_{DMSO}, compared to S-DG_{Water}, possibly due to the incorporation of more S atoms. Both 'd' and 'τ' were listed in Table S1 for the two materials. A weak peak was observed in 2θ = 41 to 43 which was due to the 010 plane of the graphite.[27]

$$n\lambda = 2d\sin\theta \quad \text{.....Equation (1)}$$

$$\tau = \frac{K.\lambda}{\beta.\cos\theta} \quad \text{.....Equation (2)}$$

where, n = a positive integer, λ = wavelength of the incident beam i.e. Cu-k_α, d = interlayer spacing and θ = diffraction angle, K = a dimensionless shape factor = 0.89, β = FWHM of the corresponding peak.

3.1.4. Raman

Two distinct bands were observed in the Raman spectrum of both the two S-DGs (Figure S9), near 1380 cm^{-1} (D-band) and 1590 cm^{-1} (G-band). The G peak is the result of in-plane vibrations of sp^2 bonded carbon atoms whereas the D peak arises due to out-of-plane

vibrations attributed to the presence of structural defects. The ratio of the intensities of these two bands (I_D/I_G) was 0.92 and 0.98, in S-DG_{Water} and S-DG_{DMSO} respectively, signifying a higher magnitude of disorder in the graphitic layer. Relatively less defect in S-DG_{Water} accounted for the more extent of graphitization in it,[16] compared to S-DG_{DMSO}. This was a good agreement with the corresponding correlation lengths found from P-XRD.[16]

3.1.5. BET Surface area analysis

BET adsorption-desorption curves of both of the materials exhibited hysteresis loops (Figure S10) which were associated with capillary condensation in slit-like micro-pores.[28] Micropores were observed in the FESEM images. The specific surface area (SSA) was 522.77 m^2g^{-1} and 693.27 m^2g^{-1} for S-DG_{Water} and S-DG_{DMSO} respectively, calculated from the 10-point linear plot obtained from the desorption BET curve (Figure S10, inset). Using de-Boer's thickness plot (Figure S11), the micropore area was evaluated. It was observed that the contribution of the total surface area mostly came from micropores for both of the materials. For S-DG_{Water}, 66.05% of the surface coverage was due to micropore area (345.28 m^2g^{-1}) while in S-DG_{DMSO}, it was 70.79% (490.79 m^2g^{-1}). Micropore volume was calculated as 0.326 $cc.g^{-1}$ and 0.663 $cc.g^{-1}$ respectively. All the obtained results from surface area and porosimetry analysis were listed in Table S2.

3.1.6. XPS

From XPS, the chemical composition of the S-DG_{Water} and S-DG_{DMSO} was estimated through elemental analysis (Table S3) according to the sensitivity factors of C, O, and S. Atomic percentage of S was found 7.02 for S-DG_{DMSO} while in S-DG_{Water} it was 3.81%. To our best knowledge, 7.02% is the highest S-load at any graphite material reported so far where any laboratory chemical has been used as the precursor. (Highest S contain: 8.102%, derived from gingko leave after prolonged process[20])

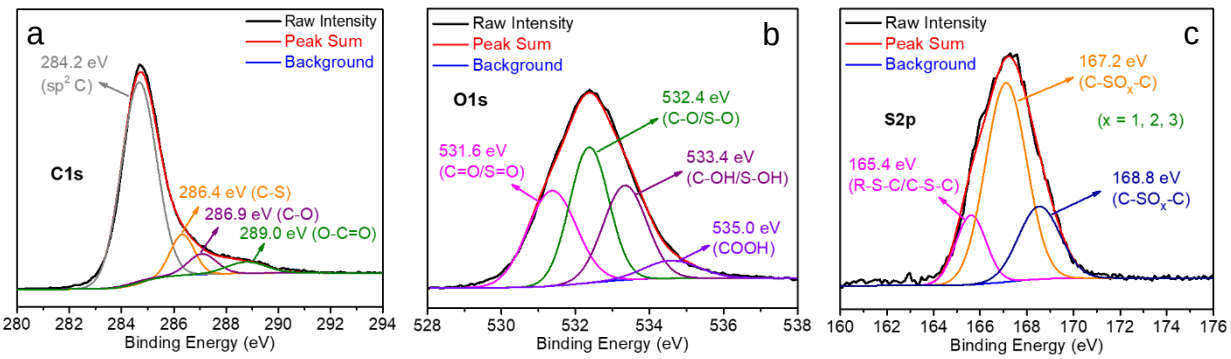

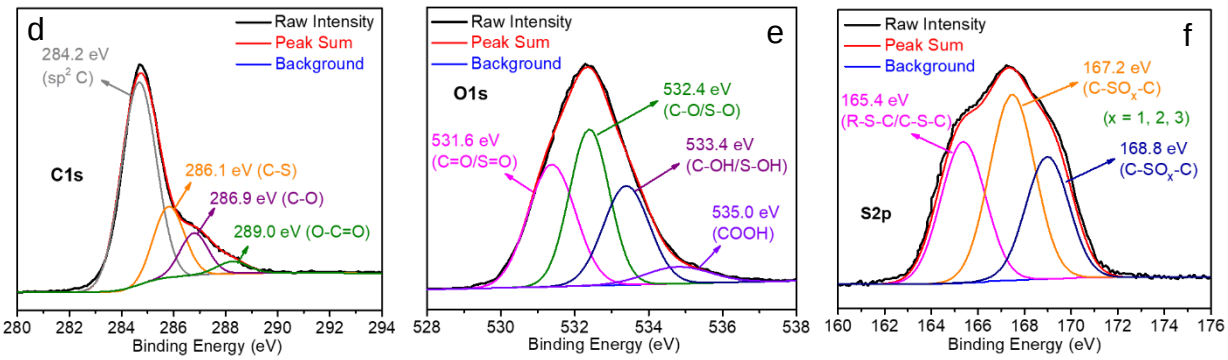

Figure 3. Deconvoluted XPS peaks of the functional groups present in each element for (a) to (c) S-DG_{Water} and (d) to (f) S-DG_{DMSO}.

All the elemental peaks (2 × 3) were deconvoluted with XPS-peak software using Gaussian peak shape followed by unbiased curve-fitting (Figure 3). The contribution of the functional groups, assigned from literature, was calculated from the corresponding peak areas through OriginLab software and listed in Table 1.

The major occupancy of sp^2-bonded carbon in both of the S-DGs was the confirmatory signature of the graphitic nature of the materials (Figure 3a, 3d).[22] Deconvoluted spectrum of the S (Figure 3c, 3f) showed the presence of three functional groups. One peak at lower binding energy (B.E.) region, 165.4 eV, was attributed to R-S-C or C-S-C group (R = alkyl or aryl).[15, 17, 29] According to the report of Zhang *et al.* this might be due to the thiophene group.[30] Other two peaks at 167.2 eV and 168.8 eV attributed to the oxidised groups of S, denoted by '-C-SO_x-C-' where x = 1, 2, 3, etc.[29] Based on the literature reports, the '-SO_x' functionality could be present in the graphitic framework in the forms of -C-SO_x-C, -R-SO_x-C, -R-SO_x-R, -O-S(O)-R, etc.[15, 18, 30] No elemental peak for S was observed at 164 eV signifying that, all the S atoms were existing as covalently attached to C or O or both and this result is consistent with HRTEM analysis.[26] Highest oxidised form of S, S^{6+}, was absent in both of the materials as no peak beyond 170 eV was found.[18, 20, 30]

Table 1. Relative percentages of the functional groups obtained from XPS study.

S-DG_{Water}

C		O		S	
Group	Contribution	Group	Contribution	Group	Contribution
C=C	74.56%	C=O/S=O	29.29%	R-S-C/ C-S-C	15.56%

C-S	13.74%	C-O/S-O	35.48%	C-SO_x-C at 167.2 eV	60.66%
C=O	6.57%	C-OH/S-OH	27.54%	C-SO_x-C at 168.8 eV	23.78%
O-C=O	5.13%	COOH	7.69%		

S-DG_{DMSO}

C		O		S	
Group	Contribution	Group	Contribution	Group	Contribution
C=C	61.03%	C=O/S=O	32.77%	R-S-C/ C-S-C	32.25%
C-S	22.06%	C-O/S-O	35.88%	C-SO_x-C at 167.2 eV	40.27%
C=O	12.94%	C-OH	25.83%	C-SO_x-C at 168.8 eV	27.48%
O-C=O	3.96%	COOH	6.22%		

Quantification of the functional groups from the deconvoluted spectrum of S2p revealed the hefty increase of C-S functionality in S-DG_{DMSO} (32.25%) compared to S-DG_{Water} (15.56%). The same feature could be correlated in the deconvoluted spectrum of C1s at 286.1 eV (13.74% to 22.06%). Total contribution of the two '-SO_x-' groups is larger than 'C-S' group in both of the materials.

3.2. Application of S-DG_{Water} and S-DG_{DMSO} as electrode materials

3.2.1. Cyclic Voltammetry (CV)

Cyclic voltammetry (CV) was performed to evaluate the supercapacitor performance of S-DG_{Water} and S-DG_{DMSO}. As shown in Figures 4a and 4b, both of the cyclic voltammograms looked quasi-rectangular in shape without any redox peak, signifying EDLC-type capacitive behaviour. The scan rate was varied from 10 mVs^{-1} to 100 mVs^{-1}. Consequently, the generated current increased steadily keeping the curve-rectangularity intact, with slight distortion. This proportionality implied low Ohmic resistance and good rate capability.[9] For S-DG_{DMSO}, the mirror-image symmetry of the voltammogram was more prominent and the enclosed curve-area was larger than that of S-DG_{Water}. It suggested that more S-loading was enhancing the supercapacitor performance.[31-33] Specific capacitance, C_{Sp} was calculated using the following equation:

$$C_{Sp} = \frac{1}{2}\frac{\int I(v)dv}{\Delta V.\vartheta.m} \quad \text{..... Equation (3)}$$

Where, $\int I(v)dv$ = area integral of the enclosed CV curve (current × potential), unit: μA.V; ΔV = potential window, 1 V; ϑ = scan rate, unit: Vs^{-1}; m = mass of the active electrode material over GCE surface (0.6 μg). Final unit of C_{Sp}: Fg^{-1}.

As shown in Figure 4c, S-DG_{Water} exhibited the highest C_{Sp} value 155.61 Fg^{-1} at ϑ = 10 mVs^{-1}. It reduced to 63.33 Fg^{-1} at ϑ = 100 mVs^{-1}. For S-DG_{DMSO}, the highest C_{Sp} value was found 261.43 Fg^{-1} at ϑ = 10 mVs^{-1} and it dropped to 147.23 Fg^{-1} at ϑ = 100 mVs^{-1}.

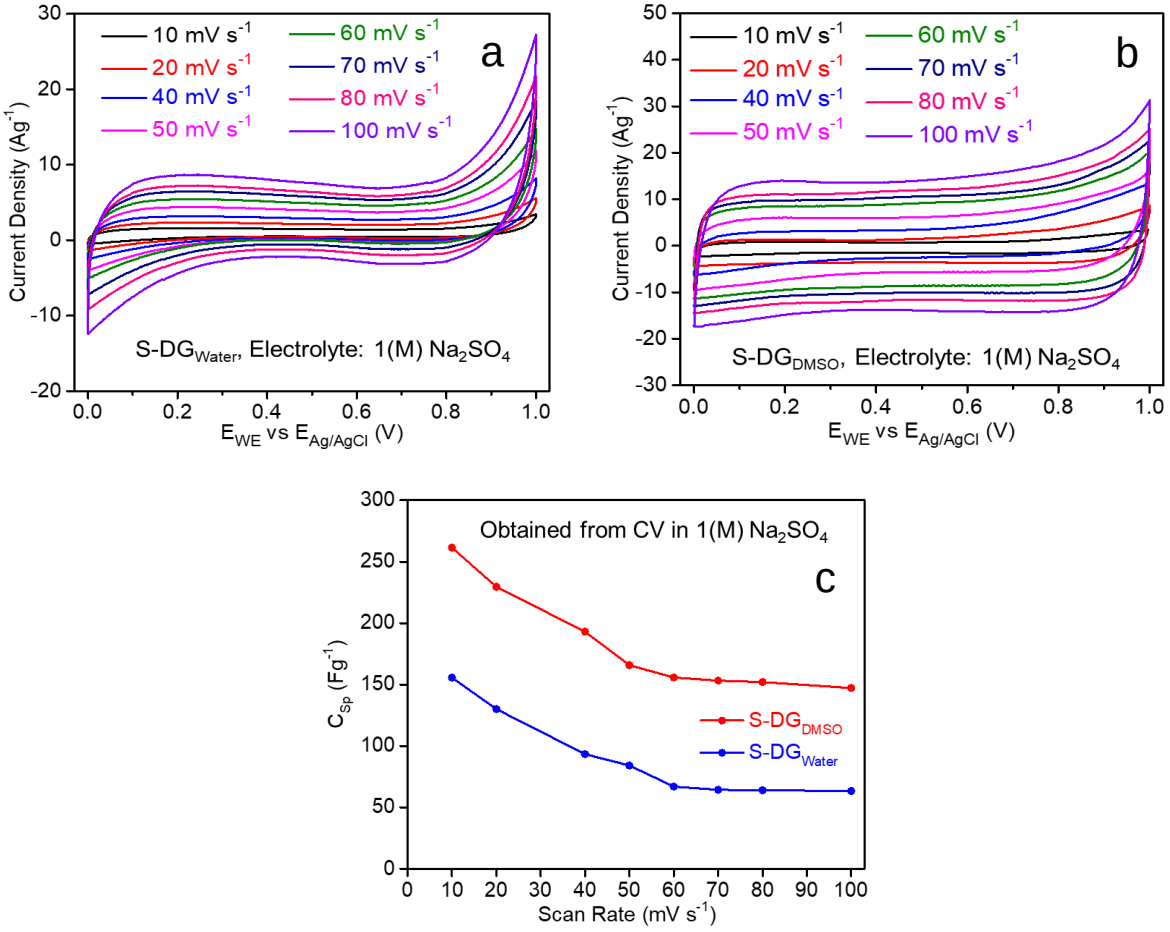

Figure 4. Performance of two S-DGs as supercapacitor electrode materials in CV using 1(M) Na_2SO_4 electrolyte within 1V potential window. (a), (b) Stacked cyclic voltammograms (current density *vs* potential) of S-DG_{Water} and S-DG_{DMSO} respectively in different scan rates; (c) Measurement of specific capacitance of two S-DGs as a function of scan rate. The current density was obtained by dividing the generated current value by 'm'.

In a porous electrode material, it is important to understand the contributions of capacitive and intercalation processes to the total amount of charges. Hence, to make a

distinction between surface-dependent capacitive charge storage (outer surface) and diffusion-driven intercalation (inner surface), Trasatti's method was employed.[34]

At a higher scan rate, the diffusion of the electrolyte ions through the electrode material is restricted due to shorter contact time. Hence, the inner surface of S-DG remains inaccessible for Na^+ and SO_4^{2-}, compared to the outer surface. At a lower scan rate, the electrolyte ions get enough time to diffuse to the inner surface of S-DG.[34] So, the total charge stored would be due to a combined effect of both the inner and outer surface of the electrode material. Figure S16a represented the inverse of specific capacitance ($1/C_{Sp}$) as a function of the square root of scan rate ($\vartheta^{1/2}$), within ϑ = 10-100 mVs^{-1}. C_{Sp} at a very slow scan rate was determined from the intercept of the straight line, which was equal to 862.07 Fg^{-1} for $S\text{-}DG_{Water}$ and 442.5 Fg^{-1} for $S\text{-}DG_{DMSO}$. Further, to get an estimation of the surface-governed capacitance, C_{Sp} was plotted against the inverse of the square root of scan rate ($\vartheta^{-1/2}$) in Figure S16b. the obtained values from the intercepts were 19.48 Fg^{-1} for $S\text{-}DG_{Water}$ and 90.23 Fg^{-1} for $S\text{-}DG_{DMSO}$. These two corresponded to 2.3% and 20.4% contribution of the surface-governed capacitance to the total C_{Sp}. This was possibly due to more S functionalities in $S\text{-}DG_{DMSO}$ than $S\text{-}DG_{Water}$ (Table S4). The rest 97.7% (in $S\text{-}DG_{Water}$) and 79.6% (in $S\text{-}DG_{DMSO}$) contribution to the total capacitance was due to diffusion of the electrolyte to the inner surface of the electrode materials. Surface contribution for $S\text{-}DG_{DMSO}$ was found to be more than that for $S\text{-}DG_{Water}$. This signified that most of the extra S atoms in $S\text{-}DG_{DMSO}$ were distributed over the graphitic surface rather than intercalating the graphitic layers. This was consistent with the elemental mapping of S (Figure 2h).

3.2.2. Galvanostatic Charging-Discharging (GCD)

Galvanostatic charging-discharging (GCD) was carried out to estimate the C_{Sp} and cyclic stability of the electrode materials. A constant current was applied within 1V potential and the required time for periodic charging and discharging was noted. The current density was varied from 3.33 Ag^{-1} to 10 Ag^{-1}. Specific capacitance, C_{Sp}, was calculated using Equation 4.

$$C_{Sp} = \frac{1}{2}\frac{I.\Delta t}{\Delta V.m} \quad \text{..... Equation (4)}$$

Where, Δt = discharging time, unit: s. Other parameters are as follows in Equation 3.

Both the GCD curves exhibited linear and nearly isosceles triangles due to stable and reversible charging-discharging (Figure 5).[15] The triangles obtained from charging-discharging of $S\text{-}DG_{DMSO}$ (Figure 5b) were more symmetrical than $S\text{-}DG_{Water}$ (Figure 5a), indicating S-

DG_{DMSO} is a better EDLC material.[5, 20] In addition, no voltage drop was observed due to internal resistance drop (IR drop) at initial discharge curve, signifying good capacitive behaviour of the materials. C_{Sp} obtained at 3.33 Ag^{-1} current density was 141.0 Fg^{-1} for S-DG_{Water} and 240.24 Fg^{-1} for S-DG_{DMSO} respectively. This value decreased almost linearly with the increasing current density because the higher current density restricted the diffusion of electrolyte ions at the micropores of S-DG. At 10 Ag^{-1} current density, C_{Sp} was obtained as 87.0 Fg^{-1} and 146.1 Fg^{-1} for S-DG_{Water} and S-DG_{DMSO} respectively (Figure 5c). At lower current density, the negligible contribution of Faradaic current resulted in little deviation from the symmetric nature of the GCD curves.[31] Higher current density overcame the appearance of this Faradaic current due to less diffusion. The energy density (E) and power density (P) were calculated from Equations 5 and 6. Figure 5d represented the Ragone plot of S-DG_{Water} and S-DG_{DMSO}. E was plotted as a function of P, both in logarithm scale. The units of E and P were expressed as '$Whkg^{-1}$' and 'Wkg^{-1}' respectively.

$$E = \frac{I.\Delta V.\Delta t}{2m} \quad \text{.....Equation (5)}$$

$$P = \frac{I.\Delta V}{2m} \quad \text{.....Equation (6)}$$

Where, all the terms represented conventional parameters, described earlier.

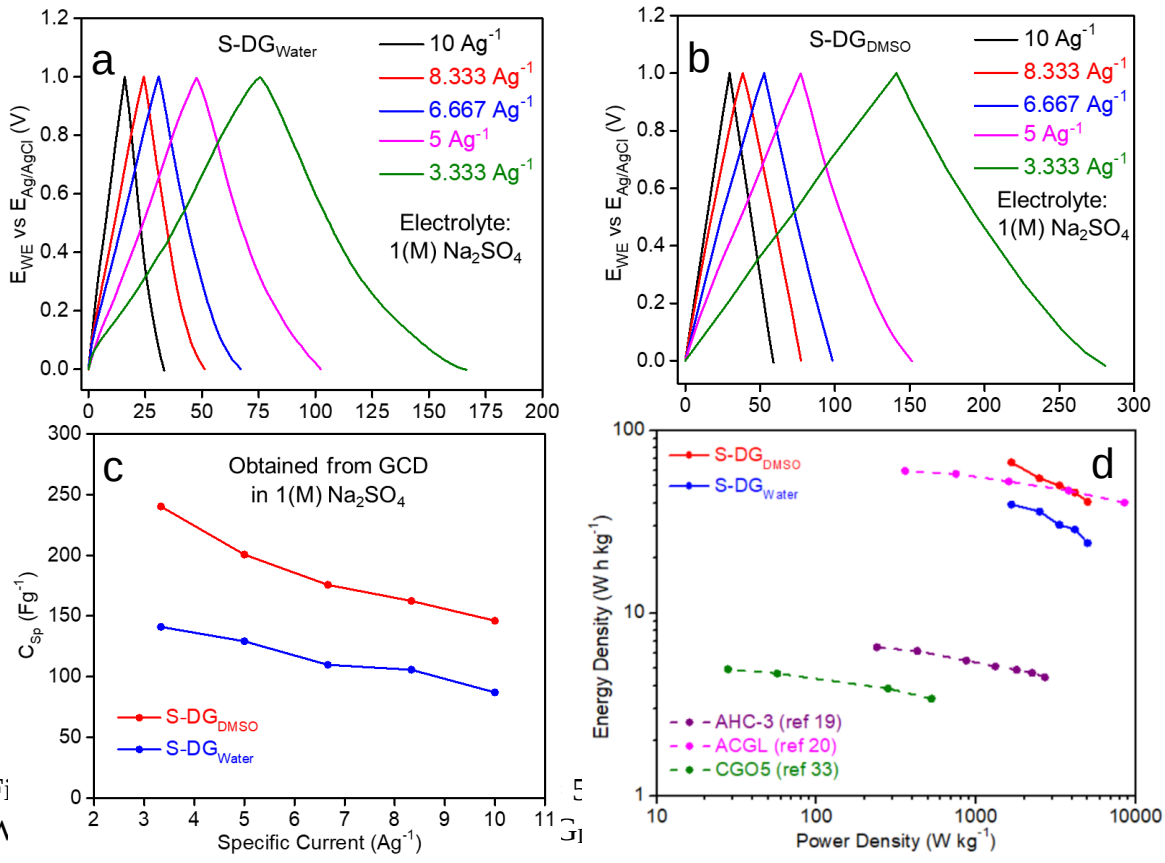

Fi [illegible] 57
W [illegible] 1;

P = 1667Wkg^{-1} when E = 66.73 Whkg^{-1}) as supercapacitor electrode materials in GCD using 1(M) Na_2SO_4 electrolyte within 1V potential window in different current densities, (c) Measurement of specific capacitance of two S-DGs as a function of specific current. (d) Ragone plots of the two S-DGs with comparison to similar electrode materials in three electrode system (solid line represented this report and dashed line represented reports from literature)

The charging-discharging phenomenon of both the materials was subjected to 10000 cycles in the same experimental condition (current density: 10 Ag^{-1}) to check their cyclic stability. Specific capacitance after every 1000 cycles was calculated from equation 4 and the capacitance retention was plotted against the number of cycles (Figure S17). In the inset, GCD curves of the last five cycles were displayed. Both of the materials retained C_{Sp} almost intact even after 10000 cycles. In close comparison between the two, S-DG_{DMSO} showed better cyclic stability (98.8% retention) than S-DG_{Water} (98.0% retention).

3.3.3. Electrochemical Impedance Spectroscopy (EIS)

Electrochemical impedance spectroscopy (EIS) was carried out to get a clearer interpretation of the charge-transfer kinetics of electrochemical behaviour for both the electrode-electrolyte combination. Nyquist plots for the electrode materials were presented in Figure S18 where the imaginary part of the impedance ($-Z_{imag}$) was plotted as a function of its real part (Z_{real}).

From the Nyquist plot, it can be observed that the electrode showed a similar type of nature in both the electrolytes and the spectra obtained is a combination of resistive and capacitive behaviour for both the systems. The absence of any prominent semi-circular arc in the high-frequency region of the spectra signifies very little charge-transfer resistance (R_{CT}) and the minimal Ohmic contact between the electrode material and electrolyte.

The impedance spectra were further fitted using a model equivalent circuit (Figure S18c). The residual χ^2 values of ~0.04 and ~0.05 for S-DG_{DMSO} and S-DG_{Water}, respectively confirm an excellent fitting. The first impedance (R_1) represents the series resistance. The second part of the model circuit is expressed by a parallel combination of a solution, interfacial and leakage resistance (R_2), and constant phase element (Q_1) (denoting the mass capacitance).[35] This part stands for the contribution of the interfacial layer.[36] The third part, expresses the modified Randle's circuit (consisting of charge transfer resistance (R_3) and two constant phase elements (Q_2 and Q_3) which denote double layer and diffusion components, respectively). The whole modified Randle's circuit signifies charge transfer kinetics.[34] The last part consists of a constant phase element (Q_4) representing the limit capacitance.[37] All the circuit parameters are

represented in Table S5. From the table, it is quite evident that the contact and solution resistance is lower for the S-DG_{DMSO}, which indicated a better conductivity. The charge transfer resistance (R_3) was found to be 2.1 Ω and 5.3 Ω respectively, for S-DG_{DMSO} and S-$DG_{Water.}$ The minimal charge transfer resistance of the former sample represents a better charge transfer kinetics and a better storage performance.

In the model equivalent circuit, the presence of constant phase elements (CPE) arises due to the variation in potential, non-linearity, and inhomogeneity in the system. The CPE can be expressed as

$$Z=Y_0 (j\omega)^{-\alpha} \ldots\ldots\ldots\ldots \text{ Equation (7)}^{38}$$

Where, α is termed as the exponent of CPE (ω is the applied angular frequency). For α=0 the component is purely resistive and for α=1 the component is purely capacitive [When, α = 1, Y_0 = 1/C for and, when α = 0, Y_0 = R where, C and R represent the capacitance and resistance respectively]. Thus, when α tends to 1, the system is more capacitive in nature and when α tends to 0 it is more resistive. From the table of fitting parameters, the exponents corresponding to double layer and intercalation components (Q_2 and Q_3) for both the samples were found to be >0.8, which signifies that the charge transfer kinetics is dominated by capacitive component.

3.3.4. CV and GCD with acid and base electrolytes

The electrochemical performance of S-DG_{DMSO} was examined in 1(M) H_2SO_4 and 1.5(M) NaOH, more current was generated in both of the cases, than 1(M) Na_2SO_4 electrolyte (Figure S19a, S19b). The highest C_{Sp} was obtained as 337.16 Fg^{-1} and 280.06 Fg^{-1} in 1(M) H_2SO_4 and 1.5 (M) NaOH respectively, at 10 mVs^{-1} scan rate (Figure S19c). In GCD, the same was calculated as 287.78 Fg^{-1} and 280.06 Fg^{-1} in 1(M) H_2SO_4 and 1.5 (M) NaOH respectively, at 3.33 Ag^{-1} current density (Figure S19d). However, in either of the electrolytes, the CV and GCD curves imparted pseudocapacitive behaviour of the material as two distinct reversible peaks were observed in the cyclic voltammograms of S-DG_{DMSO} in acid and base medium (Figure S19a, S19b) and the triangles in the charging-discharging profiles are not exactly symmetrical (Figure S19c, S19d). The charging-discharging was subjected to 10000 cycles in both of the electrolytes. The cyclic stability of S-DG_{DMSO} followed the trend: 1(M) Na_2SO_4> 1(M) H_2SO_4> 1.5(M) NaOH. Better performance in H_2SO_4 medium over NaOH medium was consistent with the more contribution of -C-SO_x-C- group than -C-S-C- (Table 1).

The highest C_{Sp} values of other S-doped graphitic materials were compared to S-DG_{DMSO} in Table 2. 2D materials, having larger surface area, certainly showed better performance compared to 3D materials. However, S-DG_{DMSO} was found to be more efficient than almost all the reported materials. Moreover, a distinctly shorter synthetic scheme of S-DG_{DMSO} is also noteworthy.

Table 2. Comparison for maximum C_{Sp} (gravimetric) values of S-doped PCM

Material	Steps[ֆ] and time required for the synthesis	Max C_{Sp} (Fg^{-1})	ESC type	Electrolyte	Ref
N, S co-doped ordered mesoporous carbon	5 steps, more than 13 hours	184	EDLC	2(M) KOH	13
S-doped exfoliated graphene[§]	Minimum 4 steps and 10 hours	320	PC	3(M) KOH	15
S-doped mesoporous carbon	5 steps and almost 6 days	191	PC	1(M) KOH	17
S-functionalized graphene aerogel	6 steps, time not mentioned properly, but too lengthy	1089	PC	6(M) KOH	18
N, S co-doped activated carbon, human hair	3 steps, more than 1 day	264	PC	6(M) KOH	19
S-doped porous carbon nanosheet	4 steps, more than 1 day	312	PC	6(M) KOH	26
S-containing activated carbon	4 steps, more than 1 day	195 240	EDLC PC	6(M) LiCl 1(M) HCl	32
S-doped micro/ mesoporous carbon-graphene composite[#]	5 steps including GO synthesis, more than 2 days	110	EDLC + PC	6(M) KOH	33
S-DG_{DMSO}	4 steps including the synthesis of	261.43	EDLC	1(M) Na_2SO_4	This work

	diazonium salt, ~7 hours	337.16	PC	1(M) H_2SO_4	
		280.06	PC	1.5(M) NaOH	

[§]2D material [#]combination of 2D and 3D materials [ֆ]Steps for reaction, deposition, or growth is considered only. Steps for filtration, washing, sonication, and drying are not included

3.3. Mechanistic understanding of EDLC-type behaviour of S-DG

The electrochemical behaviour of the S-doped graphitic material is dependent on the distribution of the S-containing functional groups into graphite and the choice of electrolyte. S has a wide range of oxidation states, from +6 to -2. Hence, its presence can give rise to both electron-rich and electron-deficient regions inside graphite.

Generally, the oxidised groups of S increase the pseudocapacitance of PCM through participating in redox reactions.[15-20] Alkaline solutions are mostly used as the electrolyte (Table 2) for the facile generation of small and fast-moving hydroxyl ion (OH^-).[17-18] In presence of a base, -SO_x groups were reduced and the pseudocapacitive current was generated.[17] Gu *et al.* showed that, in presence of an acidic electrolyte (1M H_2SO_4), reduction of the '-SO_x' groups of S-containing activated carbon took place and distinct redox peaks appeared at voltammogram.[32] They had varied the electrolyte from strong acid to completely neutral (LiCl) and achieved 100% EDLC behaviour. Both sets of acidic and alkaline redox mechanisms were presented in Table S6. Gu *et al.* modified their material by elevating the temperature from 600^{o}C to 850^{o}C which gradually converted most of the -C-SO_x-C- to C-S and observed the ESC result shift towards better EDLC-type nature.[32] They have concluded that excess amount of C-S formed a 'sulphide bridge' at the edge of the layer. It enhanced the ion movement and minimized the unwanted redox reactions, leading towards the formation of an electrical double layer. This could not be regulated through excess -C-SO_x-C. Deng *et al.* demonstrated activated carbon (AC) enriched with -SO_x but less amount of graphitic carbon and C-S failed to produce good C_{Sp} value while porous carbon nanosheet (PCNS) with ample of sp^2-carbon network and C-S functionality but less -SO_x, imparted C_{Sp} up to 312 Fg^{-1} in 6(M) KOH electrolyte. Both AC and PCNS displayed EDLC nature with a slight deviation in the case of AC. All these results were consistent with our findings that higher C-S content over -SO_x content in S-DG_{DMSO} favours attaining better EDLC-type mechanism compared to S-DG_{water} *via* rapid ion transport without inducting unwanted redox reactions. Sulfoxides and sulfones were mostly residing inside the graphite phase and the effective electron density of the S centre may elevate

compared to the real oxidation state *via* electron transfer from adjacent carbon.[33] Therefore, sulphur at its partially reduced form in -SO_x was less likely to be reduced further in S-DG and behaves as EDLC. XPS study revealed that our material didn't contain any S(VI) oxidation state which was present in other S-doped PCM (available in the literature). This was also another advantage towards the facile formation of an electrical double layer. In addition, due to the doping of S in graphite, the adjacent C atoms turned out to be little positively charged which can improve the interface wettability.[13] Also, it has been reported in the literature that the Sulphur doping actually induces hydrophilicity in porous carbon materials.[39-41] During the electrochemical measurements, the better wettability of the sulphur doped graphitic samples provides a higher accessible surface to the electrolyte ion, and as a result, a high charge transfer kinetics was observed, which further enhances the supercapacitor behaviour.

4. Conclusion

Sulphur-doped Graphite (S-DG) was synthesized successfully in a multistep method either in water or in DMSO using cellulose as the precursor for a carbon source. Aryl cellulose xanthate was heated hydrothermally in a muffle furnace at 200 ^oC to get S-DG_{Water} (3.81 atom% S) or S-DG_{DMSO} (7.02 atom% S) leading to the formation of predominantly covalent bonds between graphite and sulphur. The specific surface area was observed to be 522.77 m^2g^{-1} for S-DG_{Water} and 693.27 m^2g^{-1} for S-DG_{DMSO}. Through a comprehensive electrochemical study, we critically analysed the supercapacitive behaviour of the two materials and investigated the origin of the charge storage mechanism at the electrode-electrolyte interface. Maximum specific capacitance (C_{Sp}) of S-DG_{Water} and S-DG_{DMSO} were obtained as 155.61 Fg^{-1} and 261.43 Fg^{-1} (at scan rate 10 mVs^{-1}) respectively. The result concluded that the extent of S-doping appeared as the key factor for controlling C_{Sp}. Higher C-S content over -SO_x content in S-DG_{DMSO} favours attaining a better EDLC-type mechanism compared to S-DG_{water} *via* rapid ion transport without inducting unwanted redox reactions. For either of the materials, the diffusion-controlled process imparted major contribution to the total C_{Sp}. However, for S-DG_{DMSO}, the surface contribution was distinctly higher (20.4%) compared to S-DG_{Water} (2.3%), possibly due to a larger specific surface area. These results demonstrate the potential use of sulphur doped graphite in energy storage systems.

Acknowledgments

SM and DB are indebted to Shiv Nadar University for providing scholarships. The authors acknowledge the High-Performance Computer (HPC) of Shiv Nadar University, Magus, for theoretical calculations.

Associated Contents

Supporting Information containing the characterizations of S-DG like TEM, P-XRD, Raman, surface area and porosimetry analysis, computational details, electrochemical measurements with H_2SO_4 and NaOH electrolyte, etc.

References

1. Wang, F.; Wu, X.; Yuan, X.; Liu, Z.; Zhang, Y.; Fu, L.; Zhu, Y.; Zhou, Q.; Wu Y.; Huang, W. Latest advances in supercapacitors: from new electrode materials to novel device designs. *Chem. Soc. Rev.* **2017**, *46*, 6816-6854.

2. Benzigar, M. R.; Dasireddy, V. D. B. C.; Guan, X.; Wu T.; Liu, G. Advances on Emerging Materials for Flexible Supercapacitors: Current Trends and Beyond. *Adv. Funct. Mater.* **2020**, *30*, 2002993.

3. Cai, X.; Ren, Q.; Sun, W.; Yang, F. High-performance activated carbons for supercapacitor: Effects of porous structures, heteroatom doping, and morphology. *Int. J. Energy Res.* **2021**, *45*, 21414 - 21434.

4. Wang, S.; Liu, R.; Han, C.; Wang, J.; Li, M.; Yao, J.; Li, H.; Wang, Y. A novel strategy to synthesize hierarchical, porous carbohydrate-derived carbon with tunable properties. *Nanoscale* **2014**, *6*, 13510 - 13517.

5. Sun, W.; Zhang, Y.; Yang, F. Tuning electrochemical performance of carbon-sphere-based supercapacitors by compressive tests. *Electrochim. Acta* **2020**, *357*, 136874.

6. Wang, S.; Sun, W.; Yang, D-S.; Yang, F. Conversion of soybean waste to sub-micron porous-hollow carbon spheres for supercapacitor via a reagent and template-free route. *Mater. Today Energy* **2019**, *13*, 50-55.

7. Sun, W.; Xiao, Y.; Ren, Q.; Yang, F. Soybean-waste-derived activated porous carbons for electrochemical double-layer supercapacitors: Effects of processing parameters. *J. Energy Storage* **2020**, 27, 101070.

8. Larkins, G.; Vlasov, Y.; Holland, K. Evidence of superconductivity in doped graphite and graphene. *Supercond. Sci. Technol.* **2016**, *29*, 015015.

9. Han, J.; Zhang, L. L.; Lee, S.; Oh, J.; Lee, K.-S.; Potts, J. R.; Ji, J.; Zhao, X.; Ruoff, R. S.; Park, S. Generation of B-doped graphene nanoplatelets Uusing a solution process and their supercapacitor applications. *ACS Nano* **2013**, *7*, 19-26.

10. Jeong, H. M.; Lee, J. W.; Shin, W. H.; Choi, Y. J.; Shin, H. J.; Kang, J. K.; Choi, J. W. Nitrogen-Doped Graphene for High-Performance Ultracapacitors and the importance of Nitrogen-doped sites at basal planes. *Nano Lett.* **2011**, *11*, 2472-2477.

11. Lee, Y.; An, G. Synergistic Effects of Phosphorus and Boron co-incorporated activated carbon for ultrafast zinc-ion hybrid supercapacitors. *ACS Appl. Mater. Interfaces,* **2020**, *12*, 41342-41349.

12. Abbas, Q.; Raza, R.; Shabbir, I.; Olabi, A. G. Heteroatom doped high porosity carbon nanomaterials as electrodes for energy storage in electrochemical capacitors: A review. *J Sci: Adv. Mater. Dev.* **2019**, *4*, 341-359.

13. Zhang, D.; Hao, Y.; Zheng, L.; Ma, Y.; Feng, H.; Luo, H. Nitrogen and sulfur co-doped ordered mesoporous carbon with enhanced electrochemical capacitance performance. *J. Mater. Chem. A* **2013**, *1*, 7584-7591.

14. Hamed, A.; Hessein, A.; El-Moneim, A. A. Towards high performance flexible planar supercapacitors: In-situ laser scribing doping and reduction of graphene oxide films. *Appl. Surf. Sci.* **2021**, *551*, 149457.

15. Parveen, N.; Ansari, M. O.; Ansari, S. A.; Cho, M. H. Simultaneous sulfur doping and exfoliation of graphene from graphite using an electrochemical method for supercapacitor electrode materials. *J. Mater. Chem. A* **2016**, *4*, 233-240.

16.. Wu, Z.-S.; Tan, Y.-Z.; Zheng, S.; Wang, S.; Parvez, K.; Qin, J.; Shi, X.; Sun, C.; Bao, X.; Feng, X.; Müllen, K. Bottom-up fabrication of sulfur-doped graphene films derived from sulfur-annulated nanographene for ultrahigh volumetric capacitance micro-supercapacitors. *J. Am. Chem. Soc.* 2017, **139**, 4506-4512.

17. Zhao, X.; Zhang, Q.; Chen, C.; Zhang, B.; Reiche, S.; Wang, A.; Zhang, T.; Schlögl, R.; Su, D. S. Aromatic sulfide, sulfoxide, and sulfone mediated mesoporous carbon monolith for use in supercapacitor. *Nano Energy* **2012**, *1*, 624-630.

18. Lee, W. S. V.; Leng, M.; Li, M. X.; Huang, X. L.; Xue, J. M. Sulphur-functionalized graphene towards high performance supercapacitor. *Nano Energy* **2015**, *12*, 250-257.

19. Si, W.; Zhoua, J.; Zhanga, S.; Li, S.; Xinga W.; Zhuo, S. Tunable N-doped or dual N, S-doped activated hydrothermal carbons derived from human hair and glucose for supercapacitor applications. *Electrochim. Acta,* **2013**, *107*, 397-405.

20. Hao, E.; Liu, W.; Liu, S.; Zhang, Y.; Wang, H.; Chen, S.; Cheng, F.; Zhao, S.; Yang, H. Rich sulfur doped porous carbon materials derived from ginkgo leaves for multiple electrochemical energy storage devices. *J. Mater. Chem. A* **2017**, *5*, 2204-2214.

21. Lin, Y.; Chen, H.; Shi, Y.; Wang, G.; Chen, L.; Wang, F.; Li, S.; Yu, F.; Zhang, L. Nitrogen and sulfur co-doped graphene-like carbon from industrial dye wastewater for use as a high-performance supercapacitor electrode. *Global Challenges* **2019**, *3*, 1900043.

22. Manian, A. P.; Pham, T.; Bechtold, T. *Handbook of Properties of Textile and Technical Fibres,* **2018**, *Chapter 10*, 329-343.

23. Wang, Z. *Comprehensive Organic Name Reactions and Reagents*, **2010**, *Chapter 391*, 17423-1746.

24. Quan, B.; Yu, S.; Chung, D. Y.; Jin, A.; Park, J. H.; Sung, Y.; Piao, Y. Single source precursor-based solvothermal synthesis of heteroatom-doped graphene and its energy storage and conversion applications. *Sci. rep.* **2014**, *4*, 5639.

25. Liebert, T. *Cellulose Solvents: For Analysis, Shaping and Chemical Modification,* **2010**, *Chapter 1*, 3-54.

26. Li, G.; Sun, J.; Hou, W.; Jiang, S.; Huang, Y.; Geng, J. Three-dimensional porous carbon composites containing high-sulphur nanoparticle content for high performance for lithium-sulphur batteries. *Nat. Commun.* **2016**, *7*, 10601.

27. Deng, W.; Zhang, T.; Yang, L.; Tan, Y.; Ma, M.; Xie, X. Sulfur-doped porous carbon nanosheets as an advanced electrode material for supercapacitors. *RSC Adv.* **2015**, 5, 13046-13051.

28. Lingling, Q.; Xu, T.; Zhaofeng, W.; Xinshan, P. Pore characterization of different types of coal from coal and gas outburst disaster sites using low temperature nitrogen adsorption approach. *Int. J. Min. Sci. Technol.* **2017**, *27*, 371-377.

29. Abdelkader-Fernández, V. K.; Domingo-García, M.; J.López-Garzón, F.; Fernades, D. M.; Freire, C.; de la Torre, M. D. L.; Melguizo, M.; Godino-Salido, M. L.; Perez-Mendoza, M. Expanding graphene properties by a simple S-doping methodology based on cold CS_2 plasma. *Carbon* **2019**, *144*, 269-279.

30. Zhang, L.; Niu, J.; Li, M.; Xia, Z. Catalytic Mechanisms of Sulfur-Doped Graphene as Efficient Oxygen Reduction Reaction Catalysts for Fuel Cells. *J. Phys. Chem.* C **2014**, *118*, 3545-3553.

31. Liu, J.; Wang, X.; Gao, J.; Zhang, Y.; Lu, Q.; Liu, M. Hollow porous carbon spheres with hierarchical nanoarchitecture for application of the high performance supercapacitors. *Electrochim. Acta* **2016**, *211*, 183-192.

32. Gu, W.; Sevilla, M.; Magasinski, A.; Fuertes A. B.; Yushin, G. Sulfur-containing activated carbons with greatly reduced content of bottle neck pores for double-layer capacitors: a case study for pseudocapacitance detection. *Energy Environ. Sci.* **2013**, *6*, 2465-2476.

33.Seredych, M.; Bandosz, T. J. S-doped micro/mesoporous carbon–graphene composites as efficient supercapacitors in alkaline media. *J. Mater. Chem. A* **2013**, *1*, 11717-11727.

34. Bhattacharya, G.; Fishlock, S. J.; Roy, J. S.; Pritam, A.; Banerjee, D.; Deshmukh, S.; Ghosh, S.; McLaughlin, J. A.; Roy, S. S. Effective utilization of waste red mud for high performance supercapacitor electrodes. *Global Challenges*, **2019**, *3*, 1800066.

35. Wang, W.; Guo, S.; Lee, I.; Ahmed, K.; Zhong, J.; Favors, Z.; Zaera, F.; Ozkan, M.; Ozkan, C. S. Hydrous ruthenium oxide nanoparticles anchored to graphene and carbon nanotube hybrid foam for supercapacitors. *Sci. rep.*, **2014**, *4*, 4452.

36. Choi, W.; Shin, H. -C.; Kim, J. M.; Choi, J. -Y.; Yoon, W. -S. Modeling and Applications of electrochemical impedance spectroscopy (EIS) for Llithium-ion batteries. *J. Electrochem. Sci. Technol.*, **2020**, *11*, 1-13.

37. Basri, N. H.; Deraman, M.; Suleman, M.; Nor, N. S. M.; Dolah, B. N. M.; Sahri, M. I.; Shamsudin, S. A. Energy and power of supercapacitor using carbon electrode deposited with nanoparticles nickel oxide. *Int. J. Electrochem. Sci.*, **2016**, *11*, 95-110.

38. Bhattacharya, G.; Jothiramalingam, S. K.; Srivastava, S. B.; Thomas, J. P.; Deshmukh, S.; Pobedinskas, P.; Singh, S. P.; Leung, K. T.; Bael, M. K. V.; Haenen, K.; Roy, S. S. Probing the flat band potential and effective electronic carrier density in vertically aligned nitrogen doped diamond nanorods via electrochemical method. *Electrochim. Acta* **2017**, *246*, 68-74.

39. Tan, H.; Liu, J.; Huang, G.; Qian, Y. X.; Deng**,** Y.; Chen, G. Understanding the roles of sulphur doping for enhancing of hydrophilicity and electrochemical performance of N, S co-doped Hierarchically Porous Carbon, *ACS Appl. Energy Mater.* **2018**, *1*, 5599-5608.

40. Mohapatra, D.; Dhakal, G.; Sayed, M. S.; Subramanya, B.; Shim, J.-J.; Parida, S. Sulphur doping: unique strategy to improve the supercapacitive performance of carbon nano-onions. *ACS Appl. Mater. Interfaces* **2019**, *11*, 8040-8050.

41. Sulfur-doping effects on the supercapacitive behavior of porous spherical graphene electrode derived from layered double hydroxide template. Woo-Sik Jeon, W.-S.; Kim, C. H.; Wee, J. -H.; Kim J. H.; Kim, Y. A.; Yang, C. M. *Appl. Surf. Sci.* **2021**, *558*, 149867.